JACS
JOURNAL OF THE AMERICAN CHEMICAL SOCIETY

Article

pubs.acs.org/JACS

Membrane Insertion of a Dinuclear Polypyridylruthenium(II) Complex Revealed by Solid-State NMR and Molecular Dynamics Simulation: Implications for Selective Antibacterial Activity

Daniel K. Weber,[*,†,‡] Marc-Antoine Sani,[‡] Matthew T. Downton,[†,‡] Frances Separovic,[‡] F. Richard Keene,[*,§,∥] and J. Grant Collins[⊥]

[†]Computational Biophysics, IBM Research Australia, Melbourne, VIC 3010, Australia

[‡]School of Chemistry, Bio21 Institute, University of Melbourne, Parkville, VIC 3010, Australia

[§]School of Physical Sciences, University of Adelaide, Adelaide, SA 5005, Australia

[∥]Centre for Biodiscovery & Molecular Development of Therapeutics, James Cook University, Townsville, QLD 4811, Australia

[⊥]School of Physical, Environmental and Mathematical Sciences, University of New South Wales, Australian Defence Force Academy, Canberra, ACT 2600, Australia

Supporting Information

ABSTRACT: Dinuclear polypyridylruthenium(II) complexes bridged by a flexible methylene linker have received considerable interest as potential antibacterial agents. Their potency and uptake into bacterial cells is directly modulated by the length of the bridging linker, which has implicated membrane interactions as an essential feature of their mechanism of action. In this work, a combination of molecular dynamics (MD) simulations and solid-state NMR was used to present an atomistic model of a polypyridylruthenium(II) complex bound and incorporated into a bacterial membrane model. The results of ^{31}P, ^{2}H, ^{1}H, and ^{13}C NMR studies revealed that the antibacterial $[\{Ru(phen)_2\}_2(\mu\text{-}bb_{12})]^{4+}$ complex ($Rubb_{12}$), where phen = 1,10-phenanthroline and bb_{12} = bis[4(4′-methyl-2,2′-bipyridyl)]-1,12-dodecane), incorporated into a negatively charged model bacterial membrane, but only associated with the surface of a charge-neutral model of a eukaryotic membrane. Furthermore, an inactive $[\{Ir(phen)_2\}_2(\mu\text{-}bb_{12})]^{6+}$ ($Irbb_{12}$) analogue, which is not taken up by bacterial cells, maintained only a surface-bound association with both bacterial and eukaryotic model membranes according to ^{31}P and ^{2}H NMR. The effects of $Rubb_{12}$ on ^{31}P chemical shift anisotropy and ^{2}H acyl chain order parameters for negatively charged membranes correlated with a membrane-spanning state of the complex according to MD simulation—in which the metal centers embed in the lipid head group region and the central void, created by the biconic shape of the complex, resulting in increasing disorder of lipid acyl chains and membrane-thinning. A transbilayer mechanism and membrane-spanning may be essential for the cellular uptake and antibacterial activity of this class of compounds.

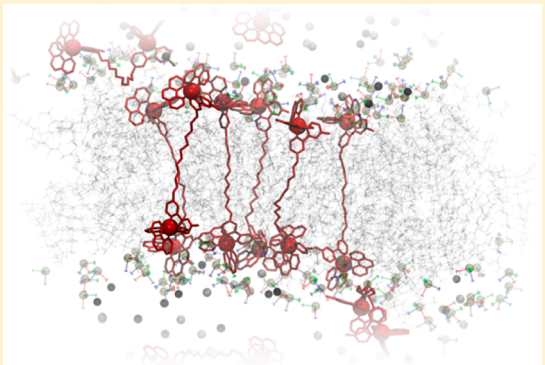

INTRODUCTION

Over the last 30 years there has been considerable interest in utilizing inert polypyridylruthenium(II) complexes as non-covalent DNA and RNA binding agents.[1−3] The ruthenium complexes can interact with nucleic acids through a variety of modes (electrostatic, intercalation, and groove binding), with the particular mode of binding being predictably governed by the metal complex structure. More recently, the antibacterial properties of the ruthenium complexes have also attracted attention.[4] While mononuclear complexes have shown good antibacterial activity, particularly against Gram-positive bacteria, dinuclear ruthenium complexes appear to show greater potential as their activity is generally maintained against antibiotic-resistant bacterial strains.[5] In particular, dinuclear polypyridylruthenium(II) complexes in which the metal centers are linked by the bis[4(4′-methyl-2,2′-bipyridyl)]-1,*n*-alkane ligand (bb_n) ($Rubb_n$, see Figure 1), show excellent antibacterial activity.[5] Although the mechanism of action is not fully understood, it has been demonstrated that the activity of the $Rubb_n$ complexes is related to the cellular uptake, with the activity of the ruthenium complexes and uptake into the bacterial cells increasing with the number of methylene groups in the bridging bb_n ligand.[6] However, while $Rubb_{12}$ is highly active, the corresponding iridium(III) complex ($Irbb_{12}$, 6+ formal charge) is totally inactive and is not taken up by the bacterial cells.[7] Furthermore, the mononuclear complex $[Ir(Me_4phen)_3]^{3+}$ (where Me_4phen = 3,4,7,8-tetramethyl-1,10-

Received: September 23, 2016
Published: October 27, 2016

DOI: 10.1021/jacs.6b09996
J. Am. Chem. Soc. 2016, 138, 15267−15277

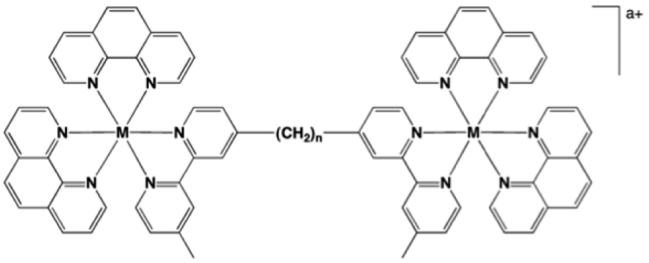

Figure 1. Structures of the inert metal complexes, $Rubb_n$ (M = Ru, a = 4) and $Irbb_n$ (M = Ir, a = 6).

phenanthroline) is also inactive and cannot cross the bacterial membrane to any significant extent,[8] whereas the ruthenium-(II) analogue, $[Ru(Me_4phen)_3]^{2+}$ shows significant activity.[6]

In this work, we have investigated the membrane interactions of $Rubb_{12}$ and $Irbb_{12}$ with phospholipid multilamellar vesicles (MLV) by ^{31}P and ^{2}H solid-state NMR, generally employed to investigate membrane interactions of antimicrobial and amyloidogenic peptides.[9−13] Changes in conformation and dynamics of the phospholipid head groups are reported through chemical shift anisotropy (CSA), spin−lattice (T_1), and spin−spin (T_2) relaxation of the ^{31}P nuclei, while changes in order of the acyl chains are determined directly from ^{2}H quadrupolar coupling constants using deuterium-labeled lipids.[14] Additional ^{1}H and ^{13}C magic angle spinning (MAS) experiments were also carried out to directly observe perturbations of lipid resonances induced by $Rubb_{12}$. Maximum-entropy magic angle spinning (MEMAS)[15] analysis of ^{31}P and "dePaking" Fourier transform[16] to resolve ^{2}H spectra were employed to precisely determine changes in model eukaryotic (neutral) and bacterial (negatively charged) membranes. The ^{31}P CSA and ^{2}H quadrupolar couplings values were subsequently used to validate long-time scale molecular dynamics (MD) simulations of multiple $Rubb_{12}$ complexes either embedded or peripherally added to phospholipid bilayer membranes.

EXPERIMENTAL SECTION

Synthesis of Metal Complexes. Dinuclear $Rubb_{12}$ and $Irbb_{12}$ complexes ΔΔ-$[\{Ru(phen)_2\}_2(\mu\text{-}bb_{12})]Cl_4$ and *rac*-$[\{Ir(phen)_2\}_2(\mu\text{-}bb_{12})](CF_3SO_3)_6$, respectively, were synthesized as reported previously.[8,17,18]

NMR Sample Preparation. NMR samples were prepared by cosolubilizing lipids (Avanti Polar Lipids, Alabaster, AL) 1,2-dimyristoyl-*sn*-glycero-3-phosphocholine (DMPC) and d_{54}-DMPC at 1:1 molar ratio, or 1,2-dimyristoyl-*sn*-glycero-3-phosphethanolamine (DMPE) and 1,2-dimyristoyl-*sn*-glycero-3-phospho-(1′-rac-glycerol) (d_{54}-DMPG) at 7:3 molar ratio, in chloroform/methanol (3:1 v/v) and drying to a thin film using a rotary evaporator. Films were suspended into deionized H_2O at ∼10 mg/mL, and after three cycles of freezing and thawing between liquid N_2 and a 60 °C water bath were aliquoted into three equal volumes and then lyophilized.

Dilute buffer volumes containing dissolved $Rubb_{12}$ or $Irbb_{12}$ were added to lipid powders (to give 50 mg/mL phospholipid), followed by vortexing, and then lyophilized. Samples were rehydrated to 70% (w/w) with Milli-Q water and freeze−thawed three times prior to measurements.

Incorporation of $Rubb_{12}$ into DMPE/DMPG (7:3) was performed by cosolubilizing the appropriate amount of DMPE, DMPG and $Rubb_{12}$ in chloroform/methanol (3:1 v/v), followed by evaporation under argon stream. The film was then dissolved in cyclohexane and lyophilized overnight. Samples were rehydrated to 70% (w/w) with buffer in D_2O and freeze−thawed three times prior to measurements. Final samples consisted of 40 mM imidazole, 110 mM KCl, 1 mM EDTA at pH 7.4 and a lipid-to-metal complex molar ratio of 10:1.

^{31}P Solid-State NMR. All solid-state experiments were conducted at either 37 or 60 °C on a Varian Inova (Palo Alto, CA) 600 MHz NMR equipped with HXY BioMAS 3.2 mm probe (Varian). ^{31}P experiments were performed at 242.76 MHz with 57 kHz SPINAL64 ^{1}H decoupling, 3 s recycle delays, 50 kHz excitation, spectral width of 125 kHz, 4096 complex points, and externally referenced to 0 ppm using H_3PO_4. Static spectra were acquired using a single-pulse experiment. All spectra were processed using NMRPipe.[19]

Chemical shift anisotropy (δ, CSA) and asymmetry (η) parameters encoded in sidebands of slow-spinning ^{31}P MAS spectra were extracted by Boltzmann-type maximum entropy (MEMAS) sideband analysis using software obtained from https://github.com/jdgehman/BS-MAS.[15] Fluid-phase systems were analyzed at 700, 1000, and 1200 Hz spinning speeds, solving for CSA values between −2 and 12 kHz in 50 Hz increments, and η values between 0 and 1 in 0.05 increments. Crystallite orientations used for matrix element calculations involved 2000 combinations of α and β angles from SIMPSON[20] crystal files and 64 γ angles uniformly dispersed over 2π.

Relaxation experiments were performed under 8 kHz MAS and fitted to a single exponential function using Gnuplot 4.6 in-built least-squares fitting functionality. ^{31}P T_1 relaxation constants were determined from a two-pulse inversion−recovery experiment, and T_2 determined from a Hahn spin−echo experiment.[21]

^{2}H Solid-State NMR. Static ^{2}H spectra utilized a solid echo sequence[22] at 92.1 MHz with 50 kHz excitation, 8192 complex points, 500 kHz spectral width, 0.5 s recycle delay, and a total echo delay of 80 μs. Pake-pattern powder spectra[23] were dePaked to resolve quadrupolar splitting at 0° orientation using weighted Fourier transformation[16] added as part of the NMRPipe 8.1 distribution.[19] Reported lipid acyl chain order parameters (S_{CD}) were calculated from ^{2}H (or D) quadrupolar splitting ($\Delta\nu_Q$) by $S_{CD} = (4/3)A_Q\Delta\nu_Q$, where A_Q is the C−D quadrupolar coupling constant of 168 kHz.[24]

^{1}H Solid-State NMR. ^{1}H MAS experiments were performed at 10 kHz spinning speed with 94 kHz proton excitation, spectral width of 125 kHz and a recycle delay of 3 s. The spectra were zero-filled to 16k points and externally referenced to 1.9 ppm using adamantane (CH protons).

^{13}C Solid-State NMR. Cross-polarization MAS at 10 kHz spinning speed with 10% proton ramp was used to prepare observable ^{13}C magnetization.[25,26] Briefly, a 94 kHz proton excitation pulse was followed by 1 ms of 45.5 kHz Hartmann−Hahn contact and 1250 complex points were acquired under 94 kHz SPINAL decoupling. A spectral window of 62.5 kHz and a recycle delay of 4 s were used. The FIDs were zero filled to 8k points and 75 Hz line broadening was applied. The spectra were externally referenced to 38.5 ppm using adamantane (CH carbons).

Molecular Dynamics Parameters. Partial charges for $Rubb_{12}$ were derived using a computationally efficient fragment-based method, in which the Δ-$[Ru(phen)_2Me_2bpy]^{2+}$ center, where Me_2bpy is 4,4′-dimethyl-2,2′-bipyridine, and decane linker were treated as discrete components in the assembly of the larger dinuclear complex (Figure 2A). By this method, various linkers may be substituted without time-consuming rederivation of charges for the metal centers. Δ-$[Ru(phen)_2Me_2bpy]^{2+}$ was constructed in UCSF Chimera[27] with the 4′-methyl of Me_2bpy capped initially by a removable CH_3 group for accurate charge-fitting, followed by geometry optimization and electrostatic potential (ESP) calculations using Gaussian09 (Rev. B.01). The B3LYP method and 6-31g* basis set was used for ligands, and LANL2DZ basis set for the ruthenium(II) center. Atom-centered partial charges were derived using restrained electrostatic potential (RESP) procedure[28] implemented in the AMBER14 distribution,[29] with intramolecular charge restraints (q = 0) applied to the capping CH_3 group (Figure 2A). RESP charges for the bridging alkyl chain were automatically generated by the R.E.D. Web server[30] with GAMESS geometry optimization of dodecane in extended conformation and intramolecular charge restraints (q = 0) applied to terminal CH_3 atoms (treated as capping groups). Two Δ-$[Ru(phen)_2Me_2bpy]^{2+}$ moieties and a bridging decane linker were then

DOI: 10.1021/jacs.6b09996
J. Am. Chem. Soc. 2016, 138, 15267−15277

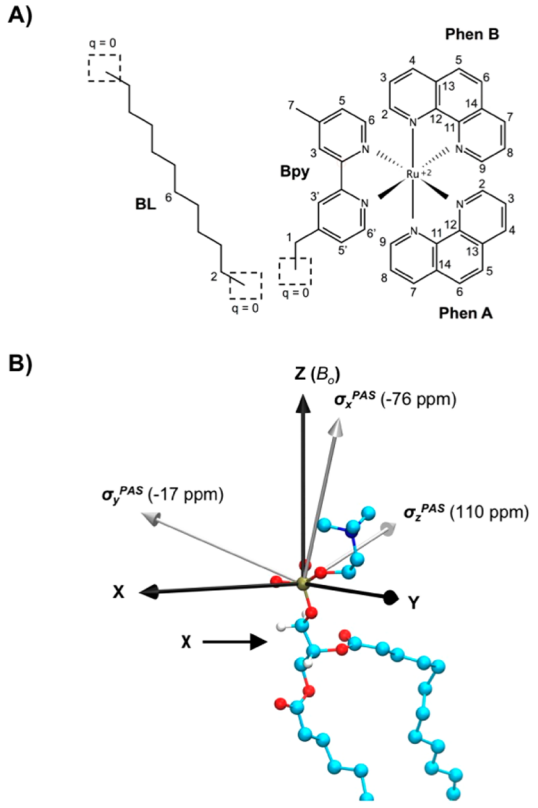

Figure 2. (A) Fragment-based RESP charge derivation scheme of a methyl-capped Δ-$[Ru(phen)_2Me_2bpy]^{2+}$ center and dodecane linker used to build the dinuclear $Rubb_{12}$ complex. (B) Example schematic of the phosphate chemical shift principal axis system components (σ_x^{PAS}, σ_y^{PAS}, and σ_z^{PAS}) of DMPC with respect to the simulation axis. The average angle of these vectors from the *Z*-axis and the order parameter of the glycerol g3 and g2 C−H bonds (marked χ) were used to determine ^{31}P CSA ($\Delta\sigma$).

bonded together following elimination of CH_3 capping groups. Noncharge parameters developed for polypyridylruthenium(II) complexes[31] were assigned to the ruthenium(II) centers and coordinating nitrogen positions, and the remaining atoms were allocated parameters from the General AMBER force field.[32] RESP charges and assigned atom types are included in Table S1 in the Supporting Information.

Molecular Dynamics Simulations. The starting bilayer of DMPE/DMPG (90:38) was generated with 64 lipids per leaflet using the CHARMM-GUI Membrane Builder.[33] Head group PE and myristoyl atoms were assigned AMBER Lipid14 parameters;[34] and PG head group parameters were taken from the Lipid11 force field.[35] Starting structures for $Rubb_{12}$-lipid simulations were constructed with 12 $Rubb_{12}$ molecules placed either peripherally, incorporated, or half-peripheral and half-incorporated into the membrane. Systems were approximated to NMR samples by hydrating to 70% (w/w) with ∼11000 TIP3P waters and, K^+ and Cl^- ions[36] added to neutralize charges from DMPG lipids and $Rubb_{12}$ complexes, respectively, and to obtain 150 mM final salt concentration.

Simulations were run using NAMD 2.10 on IBM Blue Gene/Q CPU cores. A 10 Å cutoff was applied for evaluating electrostatic and van der Waals terms, with smoothing functions disabled. Long-range electrostatics were treated using the particle mesh Ewald method, 1−3 bonded interactions ignored, 1−4 electrostatics scaled by 0.833333333 and 1−4 van der Waals potentials halved for AMBER force field compatibility. The SETTLE algorithm was applied to water hydrogen atoms and SHAKE to all other hydrogen atoms. Temperature was maintained at 333.15 K by a Langevin thermostat and damping coefficient of 5 ps^{-1}. Pressure was controlled at 1.01325 bar using the Langevin piston Nosé−Hoover method with oscillation period of 100 fs, damping time of 50 fs and anisotropic cell fluctuation. Electrostatic and bonded forces were evaluated using integration time steps of 2 fs and for all other nonbonded forces, 1 fs. Coordinates were saved every 10 ps for analysis.

Molecular Dynamics Analysis. Trajectories were analyzed according to *Z*-axis electron density profiles, lipid acyl chain order parameters and area-per-lipid measured using CPPTRAJ.[37] VMD was used for computing radial pair distribution functions, visualization[38] and execution of customized analysis scripts for calculating ^{31}P CSA values according to the method following.

In NMR of phospholipids, full width ^{31}P CSA ($\Delta\sigma$) depends on two unresolved modes of head group order: the first being the averaged orientation of the chemical shift principal axis system (σ^{PAS}, with Euler angles α and β) with respect to the magnetic field vector B_0; and the second being the order parameter, χ, of the glycerol backbone. These relate according to[13,14]

$$\Delta\sigma = \frac{3\chi}{2}[\sigma_x^{PAS}(1 - \cos^2\alpha \sin^2\beta) + \sigma_y^{PAS}(1 - \sin^2\alpha \sin^2\beta) + \sigma_z^{PAS}\sin^2\beta] \quad (1)$$

where σ_x^{PAS}, σ_y^{PAS}, and σ_z^{PAS} were taken in this work as −76, −17, and 110 ppm, respectively, as measured for analogous barium diethylphosphate (BDEP) crystals.[39] The chemical shift principal axis was defined in MD trajectories (Figure 2B) by dynamically assigning σ_y^{PAS} and σ_x^{PAS} as the average and cross product of the two nonesterified P−O bond vectors, respectively, and σ_z^{PAS} as the cross product of σ_y^{PAS} and σ_x^{PAS}. The true principal axis system was then obtained by correcting the elements with a *Z*-rotation of 9° and *X*-rotation of 13°.[39] The average angles (over all lipid and all simulation snapshots) of σ_x^{PAS}, σ_y^{PAS}, and σ_z^{PAS} from the *Z*-axis, denoted ϑ_x, ϑ_y, and ϑ_z, respectively, define Euler angles α and β by

$$\alpha = \cos^{-1}\left(\frac{\cos\vartheta_x}{\sin\vartheta_z}\right) \quad (2)$$

where $\beta = \vartheta_z$.[13]

Lastly, the order parameter χ, was determined from the average orientation of the glycerol g3 and g2 C−H bond vectors to the *Z*-axis ($\boldsymbol{\theta}_z$) by

$$\chi = -3\left\langle\frac{3\cos^2\theta_z - 1}{2}\right\rangle = -3S_{CH} \quad (3)$$

which have proven reliable and experimentally practical indicators of head group order.[40]

Dye Release Assays. Lipids, 1-palmitoyl-2-oleoyl-*sn*-glercero-3-phosphocholine (POPC), sphingomyelin (SM, porcine brain extract), 1-palmitoyl-2-oleoyl-*sn*-glercero-3-phosphoethanolamine (POPE), cardiolipin (18:1, TOCL) and 1-palmitoyl-2-oleoyl-*sn*-glercero-3-phosphoglycerol (POPG), purchased from Avanti Polar Lipids, and cholesterol (Chol; Aldrich), were used to prepare systems of POPC, POPC/SM/Chol (1:1:1 molar ratio), POPG/TOCL (3:2) and POPE/POPG (7:3 molar ratio) by cosolubilizing lipid components in chloroform/methanol (3:1) and drying to a thin film using a rotary evaporator. Lipids were resuspended into deionized water and lyophilized. Dye-loaded and dye-free large unilamellar vesicles (LUVs, 100 nm diameter) were prepared to 15 mM by suspending lipids in either dye-solution (55 mM carboxyfluorescein, 40 mM imidazole, 165 mM KOH, 1 mM EDTA) or buffer (40 mM imidazole, 110 mM KCl, 1 mM EDTA, pH 7.4), respectively, three cycles of freezing with liquid N_2 and thawing in a 40 °C water bath, then extrusion by 11 passes through a 0.1 μm polycarbonate membrane (Avanti). Dye-filled vesicles were isolated using a PD-10 gel filtration column (GE Healthcare) and lipid concentrations of eluted volumes were confirmed by total phosphorus assay.[41] All LUV systems were stored at room temperature and used within 1 week of preparation.

Dye release assays were performed in clear polystyrene 96-well (200 μL sample volume) tissue culture plates (Falcon) and increase in

DOI: 10.1021/jacs.6b09996
J. Am. Chem. Soc. 2016, 138, 15267−15277

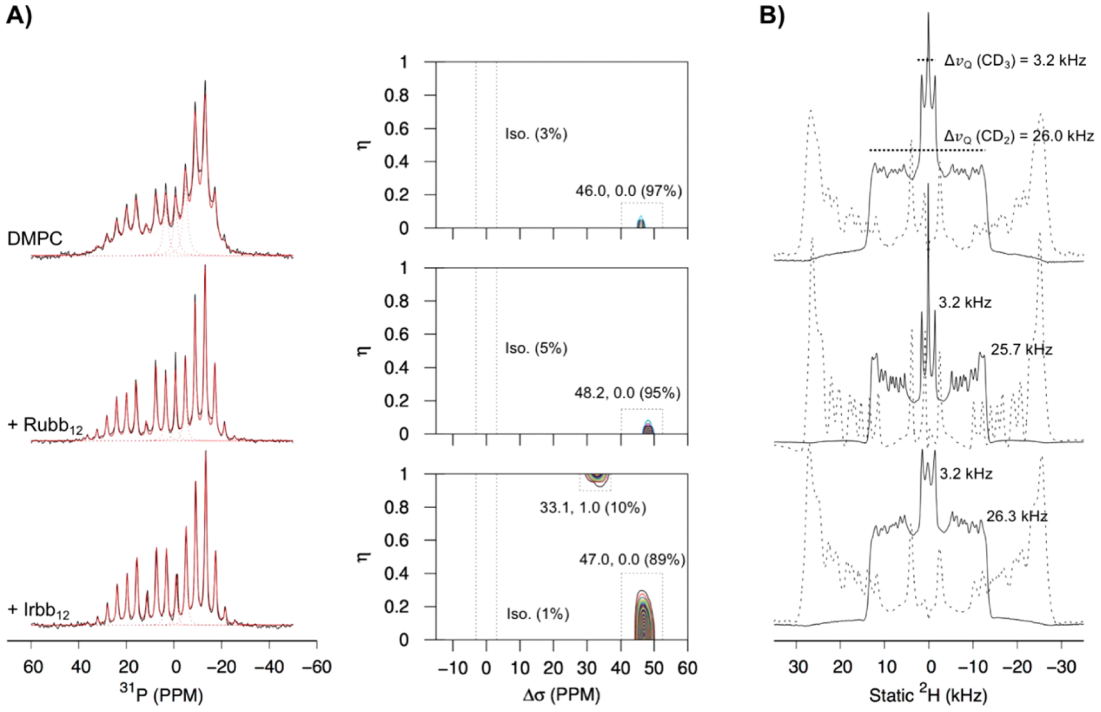

Figure 3. Solid-state (A) slow spinning ^{31}P MAS and (B) static ^{2}H NMR of DMPC/d_{54}-DMPC (1:1) MLV at 37 °C (top row) with either Rubb$_{12}$ (middle row) or Irbb$_{12}$ added at 1:10 molar ratio to phospholipid. ^{31}P η and $\Delta\sigma$ parameters were extracted from fitted MAS sideband intensities from MEMAS analysis[15] using three slow-spinning speeds (0.7, 1.0, and 1.2 kHz; only 1.0 kHz spectra are shown). The overall fits to sideband manifolds are shown as solid red lines; individual fits of the central MAS sidebands are shown for illustration (red dotted lines); and respective surface profiles of η and $\Delta\sigma$ contributions from MEMAS analysis are displayed in the middle column and annotated according to peak positions of dotted-outlined regions. Static ^{2}H spectra (B) are marked with quadrupolar couplings ($\Delta\nu_Q$) of terminal CD$_3$ deuterons and most-ordered CD$_2$ deuterons of the upper lipid acyl chain. Values of $\Delta\nu_Q$ were picked from overlaid dePaked[16] spectra (dotted line, transformed to 0° orientation and halved).

carboxyfluorescein fluorescence intensity as a result of LUV permeabilization was measured at 30 °C using a FLUOstar Optima plate reader with λ_{ex} = 492 nm excitation and λ_{em} = 520 nm emission filters and shaken prior to each measurement (one scan every 2 min for 20 min). Percentage dye release was determined from the maximal leakage induced by 0.1% Triton X-100 and subtraction of basal fluorescence intensity.

RESULTS AND DISCUSSION

Surface Association of Rubb$_{12}$ and Irbb$_{12}$ to a Fluid Zwitterionic Membrane. Perturbations to the structure and dynamics of lipid head group and acyl chains were used to determine the mode of interaction of Rubb$_{12}$ and Irbb$_{12}$ against MLV models. The ^{31}P nucleus is 100% abundant, which makes ^{31}P NMR a sensitive measure of head group perturbations through CSA, T_1 and T_2 relaxation measurements. Conversely, ^{2}H is naturally absent from lipid, but with labeling, quadrupolar coupling values, $\Delta\nu_Q$, measured by solid-state NMR reports perturbations of acyl-chain order without background from unlabeled species.

A zwitterionic DMPC/d_{54}-DMPC (1:1) MLV system was used to model eukaryotic cells, which are much less susceptible to uptake and toxicity of Rubb$_{12}$ complexes compared to bacterial cells.[42] Indeed, only mild alterations to both ^{31}P and ^{2}H Pake-pattern spectra (Figure 3) suggested Rubb$_{12}$ and Irbb$_{12}$ had limited ability to permeate through, or accumulate into, the hydrophobic acyl region of the fluid-phase (37 °C) zwitterionic system. However, surface interactions had a measurable effect on ^{31}P CSA parameters, $\Delta\sigma$ and η, extracted from sideband intensities (using 0.7 to 1.2 kHz MAS) by Boltzmann-type maximum entropy analysis (MEMAS).[15] MEMAS was developed previously as a model-free alternative to traditional least-squared fitting of static ^{31}P lineshapes, which generally suffer from having to account for isotropic chemical shift position, magnetic field-induced lipid alignment and T_2 line-broadening.

MEMAS surface plots of $\Delta\sigma$ and η contributions are depicted and annotated in Figure 3A. Rubb$_{12}$ caused small, but measurable, alteration to head group order and/or dynamics by 5% increase in $\Delta\sigma$. Similarly, Irbb$_{12}$ caused 2% increase in $\Delta\sigma$ of the main symmetric component (η = 0); however, η became more broadly distributed and a second component of 10% intensity with $\Delta\sigma$ reduced 28% and full asymmetry was suggested by MEMAS ($\Delta\sigma$ = 33.1 ppm, η = 1; Figure 3A), and maybe associated with a strongly bound population, in which lipid long-axis rotation was frozen to the NMR time scale and head group structure/order heavily affected.

^{31}P T_1 relaxation experiments, summarized in Table 1, showed that neither Rubb$_{12}$ or Irbb$_{12}$ had a measurable effect on nanosecond dynamics of DMPC head groups at 37 °C – i.e., rotations of lipid long axis and phosphate/glycerol bonds.[43] However, while Irbb$_{12}$ should have produced some alteration to T_1, as indicated by increase in η, the affected component only constituted 10% of the signal, and could not be reliably deconvoluted by multiexponential fitting to relaxation curves (see Supporting Information Figure S1 for relaxation fits). ^{31}P T_2, in contrast, doubled with Rubb$_{12}$, and increased half as much with Irbb$_{12}$, which suggested relaxation contributions from millisecond to microsecond dynamics were heavily reduced by both complexes—i.e., collective viscoelastic bilayer

DOI: 10.1021/jacs.6b09996
J. Am. Chem. Soc. 2016, 138, 15267–15277

Table 1. Summary of ^{31}P Relaxation Experiments

sample	T_1 (s)[a]	T_2 (ms)[a]
DMPC (37 °C)	0.67 ± 0.01	6.3 ± 0.3
+Rubb$_{12}$	0.67 ± 0.01	12.6 ± 0.3
+Irbb$_{12}$	0.68 ± 0.01	9.8 ± 0.4
DMPE/PG (60 °C)	0.76 ± 0.01	4.3 ± 0.2
+Rubb$_{12}$	0.76 ± 0.02	9.7 ± 0.2
+Irbb$_{12}$	0.67 ± 0.02	6.5 ± 0.2

[a] T_1 and T_2 relaxation times, with asymptotic standard errors, were calculated from MAS spectra by fitting a single exponential using Gnuplot 4.6. Fits are shown in Supporting Information Figure S1.

motions.[43] Furthermore, T_2-lengthening was also evident from sharpening of ^{31}P powder patterns (Figure 3A), which extended to lipid-acyl ^{2}H spectra only with Rubb$_{12}$ (Figure 3B).

Similar to ^{31}P powder patterns, highly convoluted unoriented ^{2}H Pake powder-pattern spectra required further processing to resolve subtle perturbations of quadrupolar couplings induced by surface-bound metal complex. In this work a weighted Fourier transformation was used to "dePake" spectra to an oriented form (i.e., a pure signal consistent with all lipids aligned parallel, or 0°, to the magnetic field). With dePaking, the maximum $\Delta\nu_Q$, which we assigned to the most-ordered CD_2 groups of the upper acyl chain, was reduced 1% by Rubb$_{12}$ but increased 1% by Irbb$_{12}$ (Figure 3B).

Rubb$_{12}$ Insertion into a Negatively Charged Bilayer. DMPE mixed with a 30% molar ratio of d_{54}-DMPG was used to model the negatively charged *E. coli* outer membrane.[44] At 37 °C, this system is between the phase transition temperatures of DMPE (50 °C) and DMPG (23 °C), and heating to 60 °C was required to obtain fluid-phase NMR spectra (Figure 4). Similar to DMPC, both Rubb$_{12}$ and Irbb$_{12}$ caused detectable head group alterations reflected by changes in ^{31}P NMR $\Delta\sigma$ and η components (Figure 4A). However, only with Rubb$_{12}$ was widespread disordering of the acyl region observed in ^{2}H spectra (Figure 4B), in which the upper CD_2 and terminal CD_3 positions experienced reductions of 21% and 34%, respectively. These reductions are consistent with insertion of Rubb$_{12}$ into the hydrophobic interior, while Irbb$_{12}$ showed no such interaction, which is in line with bacterial uptake and toxicity observed for Rubb$_{12}$, but not for Irbb$_{12}$.[8,42,45]

Interestingly, despite dramatic perturbation of the membrane interior, ^{31}P CSA parameters were only slightly affected by Rubb$_{12}$ as reflected by only a minor +0.4 ppm increase in $\Delta\sigma$. While little change in head group structure may be inferred, further analysis of molecular dynamics simulation suggested a combination of disordering and head group reorientation could cancel net changes to $\Delta\sigma$ (detailed later). Furthermore, MEMAS analysis suggested Rubb$_{12}$ reduced heterogeneity of DMPE/DMPG ^{31}P CSA (i.e., fewer components and narrower distributions), and a discrete highly ordered population (~4%, $\Delta\sigma$ = 53.1 ppm and η = 0.2) was also observed with Rubb$_{12}$ (Figure 4A), which may be assigned to a strongly bound population of lipid with slowed axial rotation. Irbb$_{12}$ had a larger impact on head group structure compared to Rubb$_{12}$ as reflected by a 4.4 ppm increase and a broadening of $\Delta\sigma$ contributions.

Similar to their effects on fluid-phase DMPC, both complexes also caused lengthening of T_2 relaxation times, at roughly the same magnitudes (i.e., ~125% with Rubb$_{12}$ and ~50% increase with Irbb$_{12}$, Table 1), which implies that effects to millisecond bilayer dynamics were nonspecific to lipid type. Furthermore, Irbb$_{12}$ caused ~10% reduction to T_1, suggesting slight perturbation to nanosecond dynamics when associated with fluid DMPE/DMPG bilayers.

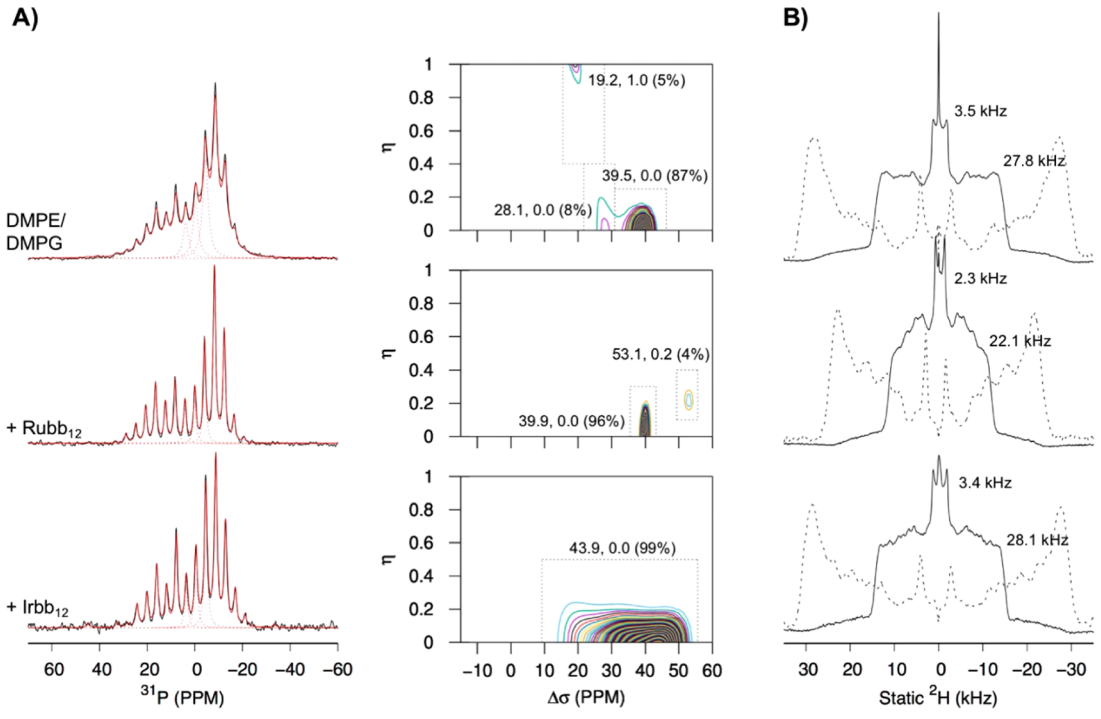

Figure 4. Solid-state (A) 1.0 kHz slow spinning ^{31}P MAS and (B) static ^{2}H NMR of DMPE/d_{54}-DMPG (7:3) at 60 °C (top row) with either Rubb$_{12}$ (middle row) or Irbb$_{12}$ (bottom row) added at 1:10 molar ratio to phospholipid. MEMAS surface profiles of ^{31}P η and $\Delta\sigma$ contributions (middle column) were calculated using sideband intensities from 0.7, 1.0, and 1.2 kHz spinning speeds. Additional details are included in the caption of Figure 3.

DOI: 10.1021/jacs.6b09996
J. Am. Chem. Soc. 2016, 138, 15267−15277

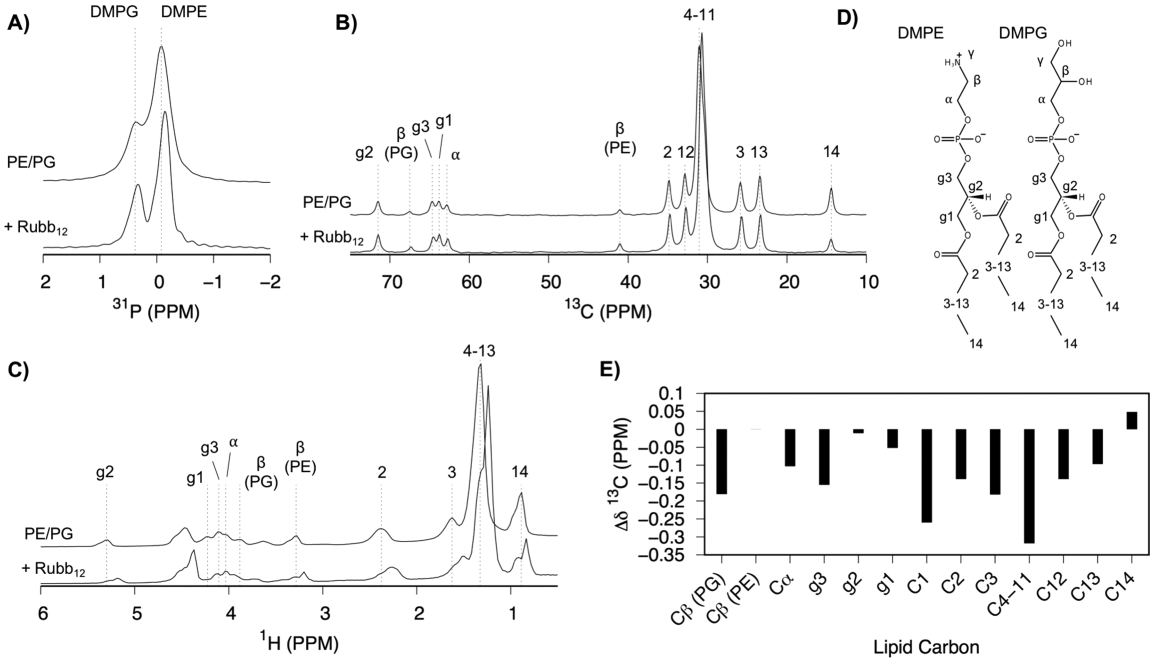

Figure 5. Solid-state (A) ^{31}P, (B) ^{13}C, and (C) ^{1}H NMR spectra of DMPE/DMPG (7:3) with Rubb$_{12}$ incorporated at 1:10 molar ratio to phospholipid. All spectra were acquired under 10 kHz MAS at 60 °C in D_2O. Acyl and head group ^{13}C/^{1}H resonances were assigned by analogy to published assignments.[48−50] (D) Lipid atom nomenclature used for NMR assignments and (E) ^{13}C chemical shift perturbations to lipid resonances upon incorporation of Rubb$_{12}$.

Table 2. Summary of Lipid Bilayer Properties Calculated from MD Simulations

measurement	DMPC[a]	DMPE/DMPG[b]			
Rubb$_{12}$ (I, E)[c]	0, 0	0, 0	0, 12	6, 6	12, 0
glycerol order, χ	0.64	0.56, 0.52	0.54, 0.59	0.49, 0.50	0.51, 0.49
ϑ_x (deg)	47	53, 52	52, 51	49, 52	46, 52
ϑ_z (deg)	70	69, 70	68, 70	67, 68	67, 68
CSA, $\Delta\sigma$ (ppm)	44	33, 32 (33)	32, 37 (33)	30, 28 (29)	33, 28 (31)
exptl[d]	46	40		40	
S_{CH}, CH_2 (max)	0.197	0.286, 0.286	0.276, 0.278	0.185, 0.174	0.142, 0.136
exptl[d]	0.206	0.221	0.175		
S_{CH}, CH_3	0.021	0.039, 0.038	0.036, 0.038	0.022, 0.018	0.016, 0.013
exptl[d]	0.025	0.028		0.018	
$D_{HG\text{-}HG}$ (Å)[e]	38	40, 43	40, 41	36, 37	33, 31
$D_{PO_4\text{–}PO_4}$ (Å)[e]	35	39, 40	39, 39	34, 36	31, 28
$D_{gly\text{–}gly}$ (Å)[e]	27	32, 32	32, 32	28, 29	25, 21
$D_{Ru\text{–}Ru}$ (Å)[e]					24

[a]Simulations of DMPC$_{128}$ were conducted at 37 °C with the same parameters used for DMPE/DMPG. Tabulated measurements are from 200 ns of equilibrated simulation. [b]Tabulated measurements were calculated individually for DMPE and DMPG lipids. Parentheses specify a weighted average measurement. [c]Rubb$_{12}$ complexes were either absent, incorporated (I) or external (E) to DMPE/DMPG in starting structures. [d]Experimental values were taken from MEMAS analyses (Figures 3B and 4B). [e]Thickness (D) at atoms constituting ethanolamine/glycerol (HG), phosphate (PO_4), backbone glycerol (gly) and [Ru(phen)$_2$(Mebpy-CH$_2$)]$^{2+}$ of incorporated Rubb$_{12}$ were calculated from electron density profiles included in Supporting Information Figure S3.

Additional ^{1}H and ^{13}C MAS experiments using non-deuterated DMPE/DMPG lipids were carried out to further characterize the interaction with Rubb$_{12}$. Diamagnetic ring currents of aromatic compounds, such as the polypyridyl ligands of Rubb$_{12}$, cause distinctive shielding/deshielding effects to nuclei within 5.5 Å,[46] and are effective in determining the position of aromatic residues of transmembrane peptides in bilayers based on selective chemical shift perturbations to lipid signals.[47] To enhance resolution, Rubb$_{12}$ was incorporated into lipids by codissolution in an organic solvent to homogenize Rubb$_{12}$ interactions throughout inner and outer MLV bilayers, rather than it being added as an aqueous solution to lyophilized lipids, as was done for ^{31}P and ^{2}H NMR studies where resolution was not as critical. Static ^{31}P spectra confirmed the lamellar phase was still obtained and $\Delta\sigma$ was unchanged after Rubb$_{12}$ incorporation. Under 10 kHz MAS, ^{31}P NMR resolved slight upfield perturbations to isotropic DMPG and DMPE signals of −0.05 and −0.07 ppm, respectively (Figure 5A). Lipids signals were well resolved in ^{13}C and ^{1}H spectra (Figure 5B and C). Chemical shift perturbations occurred throughout the entire head group and acyl region, which further supports partitioning of Rubb$_{12}$ into the hydrophobic interior of the

DOI: 10.1021/jacs.6b09996
J. Am. Chem. Soc. 2016, 138, 15267−15277

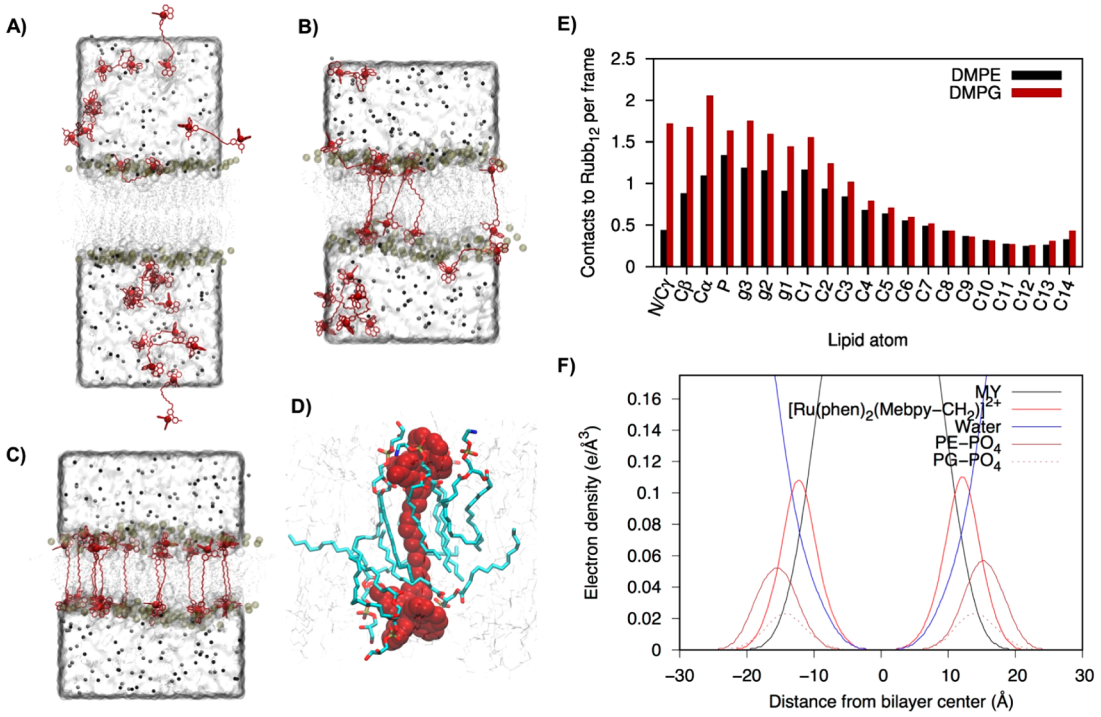

Figure 6. Molecular dynamics snapshots of 12 $Rubb_{12}$ molecules initially placed either (A) external, (B) half-inserted, and (C) fully inserted into a DMPE/DMPG (90:38) bilayer. Simulations were constructed to approximate solid-state NMR samples according to hydration (70% w/w to lipid, glass surface depiction), Na^+ ions (DMPG salt, black spheres), K^+ ions (0.15 M, black spheres) and Cl^- ions (0.15 M and $Rubb_{12}$ salt, gray spheres). Tan transparent spheres represent lipid phosphorus atoms. (D) MD snapshot of a single transmembrane $Rubb_{12}$ complex, one of 12 inserted in (C), showing surrounding lipid in direct contact with $[Ru(phen)_2(Mebpy\text{-}CH_2)]^{2+}$ centers. (E) Average number of pairwise atom−atom contacts between heavy atoms of $[Ru(phen)_2(Mebpy\text{-}CH_2)]^{2+}$ centers and selected lipid carbons within 5 Å. Average contacts are normalized by the number of carbons associated with each lipid position. (F) *Z*-axis electron density profiles of $Rubb_{12}$ fully inserted into DMPE/DMPG calculated from 200 ns of equilibrated simulation. Profiles constitute all atoms belonging to myristoyl chains (MY), $[Ru(phen)_2(Mebpy\text{-}CH_2)]^{2+}$ centers, water and phosphate ($PE{-}PO_4$ and $PG{-}PO_4$). More complete electron density profiles for systems with none and half of $Rubb_{12}$ inserted are included in Supporting Information Figure S3.

DMPE/DMPG system. Perturbations to ^1H signals were more prominent but ^{13}C NMR was able to distinguish the carbonyl C^1 position and resolve C^3, C^4, C^{12} and C^{13} positions for a more-complete perturbation profile (Figure 5E), whereby maximal upfield ^{13}C shifts occurred at DMPG Cβ, glycerol g3, carbonyl C^1 and acyl C^{4-11} carbons. 2D ^1H NOESY was also performed (Supporting Information Figure S2), and although NOESY spectra could not unambiguously resolve aromatic protons of $Rubb_{12}$, cross peaks consistent with intermolecular contacts between lipid $C^{4-13}H_2$ and $Rubb_{12}$ bpy-H3/H3′, phen A-H2, phen A/B−H3/H9, and bpy-H6/H6′ were observed. Weak cross peaks between the bridging alkyl chain and aromatic protons (bpy-H3′, bpy-H5′, phen A-H2, and phen A-H3) were observed in solution-state ROESY spectra of aqueous $Rubb_{12}$ (Supporting Information Figure S2), consequently the $Rubb_{12}$ signals from the alkane bridge could overlap with signals from lipid C^2H_2 and $C^{4-13}H_2$ in solid-state NOESY spectra. However, the well-resolved upfield bpy-H5′ showed no contacts for aliphatic protons with lipids present, which suggests that the linking chain adopted an extended conformation. Furthermore, cross peaks between bpy-H6/H6′ and CH_2 protons at 1−1.5 ppm were not observed in ROESY spectra, but were in NOESY spectra with lipid. Therefore, cross peaks between aromatic $Rubb_{12}$ ligands and aliphatic protons at 1−1.5 ppm were most likely due to intermolecular lipid contact and not intramolecular folding.

Experimental Validation of Lipid-Bilayer Simulations. The method for calculating ^{31}P CSA from MD simulations, which when combined with experimental values determined from MEMAS analysis, can provide a comprehensive description of head group conformation and order. The principle of this method is analogous to the widely used method for deriving lipid acyl order parameters, in which the angle of the C−H (or C−D) bond vector to *Z*-axis (θ) is taken to calculate the ensemble-averaged S_{CH} according to $S_{CH} = \langle 1.5\cos^2\theta - 1\rangle$, where S_{CH} may then be multiplied by $(4/3)A_Q$ (A_Q = 168 kHz) to generate the quadrupolar splitting for ^2H NMR. Similarly, ^{31}P CSA is scaled to the glycerol order parameter (χ), but also depends on the ensemble-averaged orientations of the σ_x^{PAS}, σ_y^{PAS}, and σ_z^{PAS} components of the anisotropic chemical shift tensor (Figure 2B), namely, angles ϑ_x and ϑ_z (i.e., angles of σ_x^{PAS} and σ_z^{PAS} from the Z-axis), which together with χ values are detailed in Table 2.

Using 200 ns of MD of equilibrated DMPC as a control, simulated ^{31}P CSA were within 5% of experimentally derived values: $\Delta\sigma$ = 44 ppm compared to 46 ppm (Table 2). The minor difference may be attributed to the order parameter χ = 0.64 being slightly lower than an older experimental value of 0.66,[40] but is still within a revised range of 0.6 ± 0.1,[51] while angles $\vartheta_x = 47°$ and $\vartheta_z = 70°$ fall within a range of $\vartheta_x = 55°$ and $\vartheta_z = 90°$ to $\vartheta_x = 30°$ and $\vartheta_z = 90 \pm 25°$ suggested previously.[13] Furthermore, recent evaluations of head group order parameters obtained from popular lipid force fields have described AMBER's Lipid14 force field (used in this work) as being almost within experimental error.[52] "Forking", however, which describes the known magnetic-inequivalence of the two

DOI: 10.1021/jacs.6b09996
J. Am. Chem. Soc. 2016, 138, 15267−15277

hydrogens bound at each of the g3 and g1 positions,[53] is known to be unusually large for this force field[52] and may influence our simulated ^{31}P CSA values, as g3 C−H order parameters factor into the calculation (eq 3). In addition, simulated ^{2}H acyl-tail order parameters for DMPC were within 5% of our experimentally determined values (Table 2), which is unsurprising since the Lipid14 force field has been rigorously optimized for similar measurements.[34]

Simulations involving mixed DMPE/DMPG bilayers were more complex owing to the negative charge of DMPG, and Na^+, K^+, and Cl^- ions were added to match solid-state NMR conditions. Acyl-chain order parameters of the DMPE/DMPG system were 27% and 40% greater in the upper and lower carbons, respectively (Table 2), in which the large deviations were likely to be a condensation-artifact arising from adhesion of cations to the membrane interface.[54,55] In an attempt to alleviate this effect, Na^+ ions were replaced with larger K^+ ions to reduce the depth of penetration of the positive charge.[54] An alternative method to counteract condensation of negative bilayers also includes using the larger Lennard−Jones radii of ions in the AMBER ff99 force field.[56,57] However, neither method had any effect on our DMPE/DMPG simulation, probably because smaller PE head groups are still penetrable by the larger ions. Due to inaccuracies in ion parameters, our simulations with DMPE/DMPG were used as qualitative models of our experimental NMR data.

^{31}P CSA values calculated from DMPE/DMPG simulations showed significant deviation compared to experiments − $\Delta\sigma$ = 33 ppm compared to 40 ppm (Table 2). The error appears entirely attributable to the order parameter (χ = 0.55, weighted to DMPE:DMPG lipid ratio), which is considerably lower than the expected experimental value of 0.66.[40] Chemical shift tensor angles ϑ_x = 53° and ϑ_z = 69° seem appropriate. For example, the σ_x^{PAS} component of the chemical shift tensor, which lies approximately along the head group axis (Figure 2B), was tilted on average 6° further away from the Z-axis for PE/PG compared to the PC head group (Table 2), and possibly due to greater freedom of head group motion since PE is smaller head group than PC.

Molecular Dynamics Simulations of Rubb$_{12}$ with DMPE/DMPG Bilayers. Insertion of Rubb$_{12}$ into the DMPE/DMPG membrane was evident in the solid-state ^{2}H experiments, which was further investigated by MD simulations. The availability of a generalized set of AMBER-compatible parameters for polypyridylruthenium(II) complexes[31,58] made possible simulations of 12 Rubb$_{12}$ molecules placed external, incorporated and half-external/half-incorporated relative to the membrane (Figure 6A−C). MD simulations were matched to solid-state NMR studies in terms of lipid to Rubb$_{12}$ stoichiometry, hydration level, lipid composition, temperature and salts. Convergence of the simulations were assessed by area-per-lipid values, which stabilized after 50 ns at 52.7 ± 0.9 Å^2 for lipid only, 53.6 ± 0.9 Å^2 with Rubb$_{12}$ external, 69.5 ± 1.6 Å^2 with half the Rubb$_{12}$ incorporated and 82.0 ± 1.1 Å^2 with all Rubb$_{12}$ incorporated (Supporting Information Figure S4). Rubb$_{12}$ complexes required manual insertion as spontaneous diffusion events across the membrane did not occur in the time frame simulated (250 ns). The result is not surprising as the desolvation penalty associated with diffusing a [Ru(phen)$_2$(Mebpy-CH$_2$)]$^{2+}$ center through the hydrophobic interior is estimated around +7 kJ mol^{-1} according to an experimental octanol−water partition coefficient (log P) of −2.9.[5] Such a high kinetic barrier may explain why several hours of incubation with Rubb$_n$ complexes are required for maximal toxicity and uptake into bacterial and human cell lines.[5,6,59] Observation of diffusion would likely require biased simulations, which are outside the scope of this work, and may also proceed via less energetically costly mechanisms, such as deformation of the membrane[60,61] to preserve the hydration shell of the Rubb$_{12}$ centers. Furthermore, it is noteworthy that Rubb$_{12}$ complexes were observed to cycle between extended and collapsed conformations, and form short-lived aggregates. Intramolecular folding has been suspected to be responsible for offsetting gains in lipophilicity from substituting Rubb$_n$ complexes with methylene linkers greater than 10 carbons.[5] In addition, aggregation, combined with collapse into triangular amphiphilic structures, may allow Rubb$_{12}$ complexes to cooperatively disrupt cylindrical lipid packing and stabilize highly curved aggregates.[62] Highly curved species were identified as intense isotropic components in static ^{31}P NMR lineshapes of gel-phase DMPC and DMPE/DMPG with Rubb$_{12}$ included (see Supporting Information Figure S5 and Table S2).

With Rubb$_{12}$ initially placed externally, a single complex was observed to bind the surface of DMPE/DMPG over the entire length of the simulation. The mode of this interaction is depicted in Figure 6A, for which the two metal centers of Rubb$_{12}$ are embedded at the level of phosphate and the alkyl linker is dipped into the hydrophobic interior of the membrane. Alterations to lipid head group and acyl chain structure were observed, which included selective ordering of PG head group χ by ∼10% and disordering of the upper and lower acyl carbons by 3% and 5%, respectively (Table 2). The head group ordering observed in simulation correlates with the experimentally observed ordered population of ∼4%, $\Delta\sigma$ = 53.1 ppm and η = 0.2 (Figure 4B). However, comparisons of $\Delta\sigma$ values with nonzero η contributions are difficult to make as MD time scales are far too short to sample microsecond to millisecond rotational dynamics that underpin η.[43]

While interfacial association of Rubb$_{12}$ to DMPE/DMPG may explain a small distinct population (4%) of ordered head groups in ^{31}P NMR spectra, the interaction does not account for large reductions in lipid acyl S_{CD} parameters observed experimentally. Nor does it explain widespread Rubb$_{12}$-induced perturbations throughout acyl ^{1}H and ^{13}C resonances in Figure 5B and C. However, with Rubb$_{12}$ (see Figure 6B and C), S_{CH} parameters fell 36% and 46% (upper and lower carbons) for half-incorporated, and 51% and 61% when all were incorporated (Table 2). These values, particularly with half incorporated, compared more favorably to S_{CD} reductions of 21% and 34% observed experimentally (see Figure 4C). Therefore, the NMR measurements were likely for DMPE/DMPG undergoing incomplete insertion of Rubb$_{12}$ when added to lipid. DMPE/DMPG would have a limited capacity for Rubb$_{12}$ as dissipation of negative charge would occur with each successive insertion event. Furthermore, incorporated Rubb$_{12}$ had distinguishable preference for contacting PG head groups in the MD simulations (see Figure 6D and E), but also caused proportionate displacement of Na^+ and K^+ from PE and PG head groups (see radial pair distributions in Figure S4). However, alleviation of condensation artifacts by ion-displacement would also contribute to S_{CH} reductions and make quantitative comparison of simulation and experiment difficult.

Incorporated Rubb$_{12}$ also appeared to slightly reduce acyl S_{CH} parameters for DMPG relative to DMPE (Table 2). Overall membrane-thinning of up to 9 Å was observed as

DOI: 10.1021/jacs.6b09996
J. Am. Chem. Soc. 2016, 138, 15267−15277

indicated by the electron density profiles of atoms constituting ethanolamine (PE)/glycerol (PG), phosphate, and backbone glycerol (Table 2 and Figure 6F). Thinning appeared to be the result of the Ru(II) metal centers of $Rubb_{12}$ (D_{Ru-Ru} = 24 Å) being insufficient to span the membrane bilayer thickness of ~40 Å at the phosphate of $Rubb_{12}$-free DMPE/DMPG. Contacts from MD placed the interaction of $[Ru(phen)_2(Mebpy\text{-}CH_2)]^{2+}$ centers central to the lipid head group phosphorus atoms (Figure 6E) and spread throughout acyl chains, in agreement with ^{13}C and ^{1}H MAS NMR (Figure 5B and C). Note, however, that MD contacts cannot be compared directly since the direction and magnitude of chemical shift perturbations depend strongly on the orientation of affected nuclei with respect to aromatic ligands of $Rubb_{12}$ (i.e., whether occupying shielding or deshielding zones). The representative model in Figure 6D highlights the local membrane structure that occurs with $Rubb_{12}$ incorporated, in which the membrane is thinned considerably to accommodate metal centers in the head group region. Thinning may be promoted by the bulkiness of the $[Ru(phen)_2(Mebpy\text{-}CH_2)]^{2+}$ centers relative to the alkyl linker, which provides $Rubb_{12}$ with biconic shape in comparison to the cylindrical shape of lipids. For example, the area occupied by a single $[Ru(phen)_2(Mebpy\text{-}CH_2)]^{2+}$ center, based on increase of area per lipid upon incorporation, was estimated at ~130 $Å^2$, which is roughly twice as much as lipid, yet $Rubb_{12}$ packs only a single chain into the hydrophobic core of the membrane. The packing void is, therefore, accommodated by increasing disorder of lipid chains—as observed experimentally by ^{2}H NMR (Figure 4B). Furthermore, positioning of the metal centers at the glycerol, which is chiral at the g2 carbon, may possibly factor into the slight gain in antibacterial activity observed for ΔΔ-$Rubb_n$ complexes over their ΛΛ-counterparts.[5]

With the bulky $Rubb_{12}$ centers occupying the glycerol region of DMPE/DMPG, perturbations to experimental ^{31}P CSA would be expected to be larger than only +0.4 ppm (Table 1). Indeed, the MD simulations suggested significant disordering of χ, which would have theoretically caused an experimentally detectable 10% reduction of $\Delta\sigma$ (−3 to −4 ppm). However, using fully inserted $Rubb_{12}$ as an example, a shift in PE orientation parameters ϑ_x (−7°) and ϑ_z (−2°) also contributed +6 and −3 ppm perturbations, respectively, to $\Delta\sigma$ (Table 2). Therefore, PE being forced upright (lower ϑ_x) by incorporated $Rubb_{12}$ may have offset $\Delta\sigma$ reductions from glycerol χ disordering.

$Rubb_{12}$ and $Irbb_{12}$ are Nonlytic against Dye-Filled Liposomes. Dye release assays of $Rubb_{12}$ and $Irbb_{12}$ against carboxyfluorescein-filled liposomes were performed to determine whether membrane lytic mechanisms might play a role in biological activity. Membrane lysis via pore-forming mechanisms has been described for antimicrobial peptides, and a possibility exists that these complexes may have analogous mechanisms of action. Figure 7 shows activity against a simplistic POPC eukaryotic model, a more complex POPC/SM/Chol (1:1:1) eukaryotic lipid "raft" model,[63] a POPG/TOCL (3:2) *Staphyloccus aureus* model,[64] and a POPE/POPG (7:3) *E. coli* model.[44] Unsaturated lipids were used exclusively to ensure fluid phases at experimental conditions. The antimicrobial pore-forming peptide, maculatin 1.1 (Mac1), was used as a positive control with potent lytic activity, as described by the concentration of Mac1 at which 50% dye leakage occurs (LC_{50}), against the negatively charged bacterial POPG/TOCL and POPE/POPG membrane mimics,[65] with

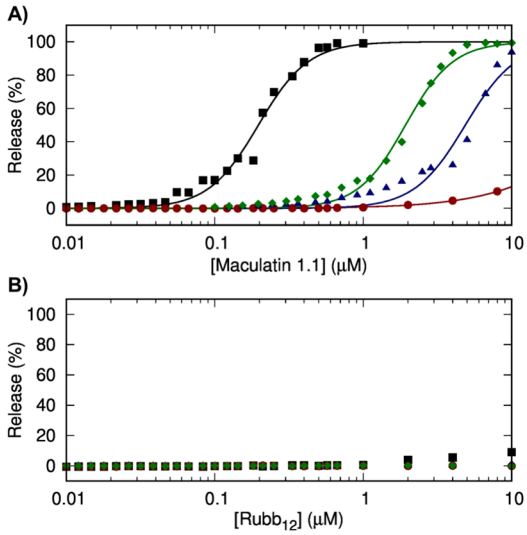

Figure 7. Dye release assays of (A) maculatin 1.1 and (B) $Rubb_{12}$ with LUV composed of POPC (black squares), POPC/SM/Chol (1:1:1; red circles), POPG/TOCL (3:2, blue triangles), and POPE/POPG (7:3; green diamonds). LUV amounted to a total concentration of 100 μM phospholipid.

LC_{50}'s of 4.9 ± 0.2 μM and 1.9 ± 0.1 μM, respectively (see Figure 7A). The activity of Mac1 against POPC (LC_{50} = 0.19 ± 0.01 μM) was considerably greater, but not against POPC/SM/Chol (LC_{50} = 46 ± 1 μM), which may be due to the ordering effect of sphingomyelin and cholesterol. In contrast, $Rubb_{12}$ and $Irbb_{12}$, which were titrated as aqueous solutions up to 1:10 molar ratio to lipid as per the stoichiometry used for NMR experiments, displayed no such activity against any of the LUVs tested, which suggests that the cytotoxic activity of these complexes may not directly involve membrane lysis. Increased permeability has, however, been described against *S. aureus*,[45] but may be due to factors not found in our model systems. Furthermore, cytotoxicity and uptake studies against mouse primary B cell and L1210 leukemia cell lines have suggested apoptotic mechanisms of cell death from mitochondrial accumulation.[59]

Roles of Membrane Permeability in Antibacterial Activity of $Rubb_n$ Complexes. Two mechanisms for antibacterial action have been identified for $Rubb_{12}$: (a) membrane permeabilization and (b) inhibition of nucleic acid-mediated (particularly RNA) processes.[42,45] The membrane interactions of $Rubb_{12}$ described in this work are obviously of primary importance to the former mechanism, while for the latter mechanism the multistep-process by which $Rubb_{12}$ permeates a membrane can be regarded as of secondary importance. Cellular uptake of $Rubb_n$ complexes is directly enhanced by increasing the length n of the bridging bb_n ligand, which in turn amplifies antibacterial activity.[5] However, enhanced uptake and activity of these complexes cannot be argued simply on grounds of lipophilicity alone. For example, the mononuclear $[Ru(Me_4phen)_3]^{2+}$ ($\log P = -1.4$)[66] and the rigid dinuclear complex $[\{Ru(phen)_2\}_2(\mu\text{-tpphz})]^{4+}$ ($\log P = -0.96$; tpphz is tetrapyridophenazine)[67] are substantially more lipophilic than $Rubb_{12}$ ($\log P = -2.9$),[5] but taken up much less readily.[6,45] Rather, the span of dinuclear complexes relative a lipid bilayer has appeared to be more relevant for influencing cellular uptake, which at shorter spans, such as $Rubb_7$ ($\log P = -3.4$), uptake is generally reduced compared to mononuclear

DOI: 10.1021/jacs.6b09996
J. Am. Chem. Soc. 2016, 138, 15267−15277

complexes, but enhanced considerably for longer species. In the current study, the importance of span is reflected by the transmembrane state uniquely adopted by $Rubb_{12}$ in a bacterial membrane model. For $Irbb_{12}$, this state was not observed, presumably due to the energetic cost of translocating a 3+ metal center across the membrane, and may explain why the complex is inactive and not taken up by bacterial cells.[7] Furthermore, the membrane-thinning occurring from incorporation of $Rubb_{12}$ also provides an explanation for the increased permeability of bacterial cells with $Rubb_n$ complexes, while $Ru(Me_4phen)_3]^{2+}$ has only been found to inhibit nucleic-acid mediated processes.[45]

CONCLUSION

Solid-state NMR of model membranes revealed that $Rubb_{12}$ inserted into a negatively charged phospholipid bilayer mimic of a bacterial membrane but not into a neutral membrane bilayer mimic of a eukaryotic membrane, while $Irbb_{12}$ maintained a surface interaction in both model systems. MD simulations directly compared lipid acyl chain and head group structural parameters obtained from NMR and showed that $Rubb_{12}$ spanned the negatively charged membrane, with the bulky metal centers situated at the glycerol backbone region and the bridging alkane linker threaded through the hydrophobic interior. Membrane-thinning occurred as a result, with the biconic shape of $Rubb_{12}$ in an extended conformation accommodated by disordering of lipid acyl chains. The transmembrane orientation of $Rubb_{12}$ in a model bacterial membrane correlates with the potent antibacterial activity of this complex. Furthermore, $Rubb_{12}$ not appearing to insert into a model eukaryotic membrane, and $Irbb_{12}$ into neither model, also fits with the relatively low toxicity observed for $Rubb_{12}$ against human cell lines and the biological inactivity of $Irbb_{12}$. Neither complex displayed lytic activity against phospholipid vesicle systems according to dye-leakage assays, which precluded a pore-forming mechanism. Insertion of $Rubb_{12}$ into bacterial membranes may be essential for antibacterial activity, either directly by modification of membrane properties (charge, fluidity/order) or as an intermediate state for uptake into the cell.

ASSOCIATED CONTENT

Supporting Information

The Supporting Information is available free of charge on the ACS Publications website at DOI: 10.1021/jacs.6b09996.

RESP partial charges and atom types assigned to $Rubb_{12}$ for MD simulation; fits to T_1 and T_2; solid-state ^1H NOESY spectra of $Rubb_{12}$ incorporated into DMPE/DMPG and solution-state ROESY spectra of $Rubb_{12}$; electron density profiles calculated from MD trajectories; area-per-lipid and radial-pair-distribution functions calculated from MD trajectories; static ^{31}P spectra and MEMAS surface profiles of gel-phase DMPC and DMPE/DMPG with $Rubb_{12}$ and $Irbb_{12}$; T_1 and T_2 relaxation times (PDF)

AUTHOR INFORMATION

Corresponding Authors

*danweb@au1.ibm.com

*richard.keene@adelaide.edu.au

Notes

The authors declare no competing financial interest.

ACKNOWLEDGMENTS

We acknowledge the Victorian Life Sciences Computing Initiative (VLSCI) for the provision of supercomputing resources, and Michael Leeming for his assistance in quantum mechanical calculations. D.K.W. was a recipient of an Australian Postgraduate Award, David Lachlan Hay Memorial Fund Writing-up Award and Dowd Foundation Postgraduate Research Scholarship.

REFERENCES

(1) Zeglis, B. M.; Pierre, V. C.; Barton, J. K. *Chem. Commun.* **2007**, *7345*, 4565.

(2) Keene, F. R.; Smith, J. A.; Collins, J. G. *Coord. Chem. Rev.* **2009**, *253*, 2021.

(3) Gill, M. R.; Thomas, J. A. *Chem. Soc. Rev.* **2012**, *41*, 3179.

(4) Li, F.; Collins, J. G.; Keene, F. R. *Chem. Soc. Rev.* **2015**, *44*, 2529.

(5) Li, F.; Mulyana, Y.; Feterl, M.; Warner, J. M.; Collins, J. G.; Keene, F. R. *Dalton Trans.* **2011**, *40*, 5032.

(6) Li, F.; Feterl, M.; Mulyana, Y.; Warner, J. M.; Collins, J. G.; Keene, F. R. *J. Antimicrob. Chemother.* **2012**, *67*, 2686.

(7) Pandrala, M.; Li, F.; Feterl, M.; Mulyana, Y.; Warner, J. M.; Wallace, L.; Keene, F. R.; Collins, J. G. *Dalton Trans.* **2013**, *42*, 4686.

(8) Pandrala, M.; Li, F.; Wallace, L.; Steel, P. J.; Moore, B., II; Autschbach, J.; Collins, J. G.; Keene, F. R. *Aust. J. Chem.* **2013**, *66*, 1065.

(9) Sani, M.-A.; Separovic, F. *J. Magn. Reson.* **2015**, *253*, 138.

(10) Sani, M.-A.; Separovic, F. In *Advances in Biological Solid-State NMR: Proteins and Membrane-Active Peptides*; Separovic, F., Naito, A., Eds.; The Royal Society of Chemistry: Cambridge, UK, 2014; pp 287–303.

(11) Weber, D. K.; Gehman, J. D.; Separovic, F.; Sani, M.-A. *Aust. J. Chem.* **2012**, *65*, 472.

(12) Gehman, J. D.; Separovic, F. In *Methods in Molecular Biology*; Hill, A. F., Barnham, K. J., Bottomley, S. P., Cappai, R., Eds.; Humana Press: Totowa, NJ, 2011; Vol. *752*, pp 165–177.

(13) Gehman, J. D.; O'Brien, C. C.; Shabanpoor, F.; Wade, J. D.; Separovic, F. *Eur. Biophys. J.* **2008**, *37*, 333.

(14) Gehman, J. D.; Separovic, F. In *Modern Magnetic Resonance*; Webb, G. A., Ed.; Springer Netherlands: Dordrecht, 2006; pp 305–311.

(15) Sani, M.-A.; Separovic, F.; Gehman, J. D. *Biophys. J.* **2011**, *100*, L40.

(16) Sani, M.-A.; Weber, D. K.; Delaglio, F.; Separovic, F.; Gehman, J. D. *PeerJ* **2013**, *1*, e30.

(17) Mulyana, Y.; Weber, D. K.; Buck, D. P.; Motti, C. A.; Collins, J. G.; Keene, F. R. *Dalton Trans.* **2011**, *40*, 1510.

(18) Morgan, J. L.; Spillane, C. B.; Smith, J. A.; Buck, D. P.; Collins, J. G.; Keene, F. R. *Dalton Trans.* **2007**, 4333.

(19) Delaglio, F.; Grzesiek, S.; Vuister, G. W.; Zhu, G.; Pfeifer, J.; Bax, A. *J. Biomol. NMR* **1995**, *6*, 277.

(20) Bak, M.; Rasmussen, J. T.; Nielsen, N. C. *J. Magn. Reson.* **2000**, *147*, 296.

(21) Hahn, E. L.; Maxwell, D. E. *Phys. Rev.* **1952**, *88*, 1070.

(22) Davis, J. H.; Jeffrey, K. R.; Bloom, M.; Valic, M. I.; Higgs, T. P. *Chem. Phys. Lett.* **1976**, *42*, 390.

(23) Pake, G. E. *J. Chem. Phys.* **1948**, *16*, 327.

(24) Burnett, L. J.; Muller, B. H. *J. Chem. Phys.* **1971**, *55*, 5829.

(25) Hartmann, S. R.; Hahn, E. L. *Phys. Rev.* **1962**, *128*, 2042.

(26) Metz, G.; Wu, X. L.; Smith, S. O. *J. Magn. Reson., Ser. A* **1994**, *110*, 219.

(27) Pettersen, E. F.; Goddard, T. D.; Huang, C. C.; Couch, G. S.; Greenblatt, D. M.; Meng, E. C.; Ferrin, T. E. *J. Comput. Chem.* **2004**, *25*, 1605.

(28) Bayly, C. I.; Cieplak, P.; Cornell, W. D.; Kollman, P. A. *J. Phys. Chem.* **1993**, *97*, 10269.

(29) Case, D. A.; Babin, V.; Berryman, J. T.; Betz, R. M.; Cai, Q.; Cerutti, D. S.; Cheatham, T. E., III; Darden, T. A.; Duke, R. E.; Gohlke, H.; Goetz, A. W.; Gusarov, S.; Homeyer, N.; Janowski, P.;

DOI: 10.1021/jacs.6b09996
J. Am. Chem. Soc. 2016, 138, 15267–15277

Kaus, J.; Kolossváry, I.; Kovalenko, A.; Lee, T. S.; LeGrand, S.; Luchko, T.; Luo, R.; Madej, B.; Merz, K. M.; Paesani, F.; Roe, D. R.; Roitberg, A.; Sagui, C.; Salomon-Ferrer, R.; Seabra, G.; Simmerling, C. L.; Smith, W.; Swails, J.; Walker, R. C.; Wang, J.; Wolf, R. M.; Wu, X.; Kollman, P. A. *AMBER14*; University of California: San Francisco, 2014.
(30) Vanquelef, E.; Simon, S.; Marquant, G.; Garcia, E.; Klimerak, G.; Delepine, J. C.; Cieplak, P.; Dupradeau, F. Y. *Nucleic Acids Res.* **2011**, *39*, W511.
(31) Brandt, P.; Norrby, T.; Åkermark, B.; Norrby, P.-O. *Inorg. Chem.* **1998**, *37*, 4120.
(32) Wang, J.; Wolf, R. M.; Caldwell, J. W.; Kollman, P. A.; Case, D. A. *J. Comput. Chem.* **2004**, *25*, 1157.
(33) Wu, E. L.; Cheng, X.; Jo, S.; Rui, H.; Song, K. C.; Davila-Contreras, E. M.; Qi, Y.; Lee, J.; Monje-Galvan, V.; Venable, R. M.; Klauda, J. B.; Im, W. *J. Comput. Chem.* **2014**, *35*, 1997.
(34) Dickson, C. J.; Madej, B. D.; Skjevik, Å. A.; Betz, R. M.; Teigen, K.; Gould, I. R.; Walker, R. C. *J. Chem. Theory Comput.* **2014**, *10*, 865.
(35) Skjevik, Å. A.; Madej, B. D.; Walker, R. C.; Teigen, K. *J. Phys. Chem. B* **2012**, *116*, 11124.
(36) Joung, I. S.; Cheatham, T. E. *J. Phys. Chem. B* **2008**, *112*, 9020.
(37) Roe, D. R.; Cheatham, T. E. *J. Chem. Theory Comput.* **2013**, *9*, 3084.
(38) Humphrey, W.; Dalke, A.; Schulten, K. *J. Mol. Graphics* **1996**, *14*, 33.
(39) Herzfeld, J.; Griffin, R. G.; Haberkorn, R. A. *Biochemistry* **1978**, *17*, 2711.
(40) Seelig, J.; Gally, H. U. *Biochemistry* **1976**, *15*, 5199.
(41) Anderson, R. L.; Davis, S. *Clin. Chim. Acta* **1982**, *121*, 111.
(42) Li, F.; Harry, E. J.; Bottomley, A. L.; Edstein, M. D.; Birrell, G. W.; Woodward, C. E.; Keene, F. R.; Collins, J. G. *Chem. Sci.* **2014**, *5*, 685.
(43) Dufourc, E. J.; Mayer, C.; Stohrer, J.; Althoff, G.; Kothe, G. *Biophys. J.* **1992**, *61*, 42.
(44) Morein, S.; Andersson, A. S.; Rilfors, L.; Lindblom, G. *J. Biol. Chem.* **1996**, *271*, 6801.
(45) Li, F.; Feterl, M.; Warner, J. M.; Keene, F. R.; Collins, J. G. *J. Antimicrob. Chemother.* **2013**, *68*, 2825.
(46) Case, D. A. *J. Biomol. NMR* **1995**, *6*, 341.
(47) de Planque, M. R. R.; Bonev, B. B.; Demmers, J. A. A.; Greathouse, D. V.; Koeppe, R. E.; Separovic, F.; Watts, A.; Killian, J. A. *Biochemistry* **2003**, *42*, 5341.
(48) Forbes, J.; Bowers, J.; Shan, X.; Moran, L.; Oldfield, E.; Moscarello, M. A. *J. Chem. Soc., Faraday Trans. 1* **1988**, *84*, 3821.
(49) Auger, M. *Curr. Opin. Mol. Biol.* **2000**, *4*, 119.
(50) Tang, M.; Waring, A. J.; Hong, M. *J. Am. Chem. Soc.* **2007**, *129*, 11438.
(51) Strenk, L. M.; Westerman, P. W.; Doane, J. W. *Biophys. J.* **1985**, *48*, 765.
(52) Botan, A.; Favela-Rosales, F.; Fuchs, P. F. J.; Javanainen, M.; Kanduč, M.; Kulig, W.; Lamberg, A.; Loison, C.; Lyubartsev, A.; Miettinen, M. S.; Monticelli, L.; Määttä, J.; Ollila, O. H. S.; Retegan, M.; Róg, T.; Santuz, H.; Tynkkynen, J. *J. Phys. Chem. B* **2015**, *119*, 15075.
(53) Gally, H. U.; Pluschke, G.; Overath, P.; Seelig, J. *Biochemistry* **1981**, *20*, 1826.
(54) Khandelia, H.; Witzke, S.; Mouritsen, O. G. *Biophys. J.* **2010**, *99*, 3887.
(55) Pastor, R. W.; MacKerell, A. D. *J. Phys. Chem. Lett.* **2011**, *2*, 1526.
(56) Aqvist, J. *J. Phys. Chem.* **1990**, *94*, 8021.
(57) Skjevik, A. A.; Madej, B. D.; Dickson, C. J.; Lin, C.; Teigen, K.; Walker, R.; Gould, I. R. *Phys. Chem. Chem. Phys.* **2016**, *18*, 10573.
(58) Reymer, A.; Norden, B. *Chem. Commun.* **2012**, *48*, 4941.
(59) Pisani, M. J.; Fromm, P. D.; Mulyana, Y.; Clarke, R. J.; Körner, H.; Heimann, K.; Collins, J. G.; Keene, F. R. *ChemMedChem* **2011**, *6*, 848.
(60) Li, L. B.; Vorobyov, I.; Allen, T. W. *Biochim. Biophys. Acta, Biomembr.* **2012**, *1818*, 135.
(61) Vorobyov, I.; Olson, T. E.; Kim, J. H.; Koeppe, R. E.; Andersen, O. S.; Allen, T. W. *Biophys. J.* **2014**, *106*, 586.
(62) Israelachvili, J. N.; Mitchell, D. J.; Ninham, B. W. *J. Chem. Soc., Faraday Trans. 2* **1976**, *72*, 1525.
(63) de Almeida, R. F. M.; Fedorov, A.; Prieto, M. *Biophys. J.* **2003**, *85*, 2406.
(64) Beining, P. R.; Huff, E.; Prescott, B.; Theodore, T. S. *J. Bacteriol.* **1975**, *121*, 137.
(65) Sani, M.-A.; Henriques, S. T.; Weber, D.; Separovic, F. *J. Biol. Chem.* **2015**, *290*, 19853.
(66) Gorle, A. K.; Feterl, M.; Warner, J. M.; Primrose, S.; Constantinoiu, C. C.; Keene, F. R.; Collins, J. G. *Chem. - Eur. J.* **2015**, *21*, 10472.
(67) Gill, M. R.; Garcia-Lara, J.; Foster, S. J.; Smythe, C.; Battaglia, G.; Thomas, J. A. *Nat. Chem.* **2009**, *1*, 662.

DOI: 10.1021/jacs.6b09996
J. Am. Chem. Soc. 2016, 138, 15267−15277